A Climatonomic Description of the Surface Energy Balance in the Central Sahel. Part I: Shortwave Radiation

ANDREW R. LARE AND SHARON E. NICHOLSON

Department of Meteorology, Florida State University, Tallahassee, Florida

(Manuscript received 3 April 1989, in final form 11 August 1989)

ABSTRACT

The climate of the West African Sahel is characterized by unusually long (multiyear) persistence of anomalously wet or dry conditions. An increasing body of evidence suggests that land surface processes contribute to this persistence and to the severity of drought. In this study, we quantify land surface characteristics and fluxes in the Sahel in order to determine the degree to which they vary in response to rainfall fluctuations and anthropogenic effects on the surface. The Lettau climatonomy model is used to assess surface energy balance near Niamey, Niger. This article presents the first of three parts of the model, shortwave radiation climatonomy. Using irradiance at the top of the atmosphere as a forcing function, the model calculates global radiation, atmospheric heating, ground-absorbed solar radiation and planetary or top albedo. Sensitivity studies show that submedium absorption of solar radiation is primarily affected by surface albedo and cloudiness; the aerosol content of the heavily dust-laden Sahel atmosphere has little effect. A comparison with time series approximating global radiation on clear and partly cloudy days shows that the model accurately assesses the clear sky case but that better cloud parameterization would improve model results.

1. Introduction

The growing perception of climate as an integral part of the global environmental system, influenced by and influencing its terrestrial and aquatic boundaries, has enhanced the need for assessing surface characteristics and the exchange of energy and matter with the atmosphere. This is particularly true for the land surface, which is increasingly acknowledged as having a major impact on climate and weather on global, regional, synoptic and mesoscales (Anthes 1984; Nicholson 1988). There exists a need to quantify surface characteristics and processes for improving numerical simulation of climate and for monitoring long-term climatic and environmental change.

The West African Sahel is a region where land surface processes appear to influence climate significantly. Drought has prevailed in the region since the 1960s and the need to understand the causes of this phenomenon provides the motivation for our current study. Charney (1975) once postulated that its origin was anthropogenic modification of the land surface, the mechanism being the impact of desertification on surface energy balance via altered surface albedo. While few scientists currently accept the notion that surface changes *caused* the drought, an increasing body of evidence suggests that land surface processes can prolong and *intensify* drought in the Sahel. The 20-year duration (Nicholson 1986, 1988), a highly unusual occurrence elsewhere, is often cited as evidence of a land–atmosphere feedback mechanism whereby droughts are self-reinforcing as a result of the land surface changes which they produce. These changes include not only albedo, but also soil moisture, evapotranspiration, surface temperature, roughness and dust generation, all of which affect the mass and energy exchange with the atmosphere.

The ultimate confirmation of this hypothesis presents a twofold problem: providing surface data for numerical simulations of the drought and monitoring the land surface and its characteristics on a regional scale. A number of GCM studies have attempted to ascertain the role of land surface processes in Sahel drought, usually modifying one variable at a time and utilizing highly unrealistic perturbations of surface parameters (e.g., Charney et al. 1977; Sud and Fennessy 1984). These studies would be enhanced by realistic assessments of the manifold land surface changes which accompany dry and wet years in the Sahel. Long-term environmental modification by people may likewise have significant impact on surface properties, and hence, surface energy balance. Environmental monitoring can be accomplished with satellite observations and recently a number of satellite methods have been applied to calculating surface fluxes and energy balance (e.g., Carlson et al. 1981; Price 1982; Taconet et al. 1986a, 1986b; Abdellaoui et al. 1986). These methods, however, provide only indirect estimates of surface parameters and must be verified with ground truth.

Corresponding author address: Andrew R. Lare, Department of Meteorology, Florida State University, Tallahassee, FL 32306-3034.

Calculations of surface energy balance have typically been the province of micro- or boundary-layer meteorology and a number of sophisticated models have been developed using conventional meteorological data as input (Monteith 1975; Deardorff 1978; Brutsaert 1982; Camillo et al. 1983). The scale of the micrometeorological models is incompatible with those required to initialize circulation models (GCMs) and verify satellite observations, our current strategies for assessing the global environment and its impact on climate. This dichotomy is recognized and to bridge this gap, field campaigns such as the HAPEX-MOBILHY experiment in France and the FIFE experiment in the Great Plains have been carried out. These were designed to determine methodologies to regionally integrate the relevant properties and fluxes in order to mesh the various time and space scales of ground-truth, satellites, and large-scale models and processes.

Pinker and Corio (1987) pointed out that the "climatonomy" model of Lettau is particularly well suited for large-scale studies and thus has applicability both to GCM studies and satellite methodologies. This model, developed by Lettau in the late 1960s (Lettau 1969; Lettau and Lettau 1969, 1975), was one of the first attempts to quantify climate and it has been tested in a number of diverse locations worldwide (e.g., Lettau 1970; Lettau and Baradas 1973; Dabberdt and Davis 1978; Lettau and Lettau 1978; Lettau et al. 1979; Kutzbach 1980; Riordan 1982). Although originally designed to be valid on climatic time scales, its applicability to the somewhat smaller time and space scales of satellite observations has been recently demonstrated (Pinker and Corio 1987; Corio and Pinker 1987).

Lettau's climatonomy scheme consists of three submodels: shortwave radiation, evapoclimatonomy and thermo-climatonomy (Table 1). The input or forcing function of the shortwave submodel is extra-atmospheric irradiance I'; the output, or response, is the planetary or top albedo A^* and the total ground absorption of solar radiation. The latter quantity is the portion of global radiation G^* that is not reflected spaceward, or $(1 - a_s)G^*$, where a_s is surface albedo. Ground absorption, $(1 - a_s)G^*$, together with precipitation rate provides input for the evapoclimatonomy submodel, which in turn predicts exchangeable soil moisture, runoff and evapotranspiration rate. The input to the thermo-climatonomy model is again $(1 - a_s)G^*$ and E, evapotranspiration. Thus, it is driven by the net shortwave contribution to surface heating minus the expenditure for latent heating of the atmosphere. Output of this submodel is sensible heat flux to the subsurface and air, all remaining fluxes of the surface energy budget including net radiation, and surface and air temperatures.

We have applied climatonomy to describing the surface energy balance at a Sahelian region near Niamey, Niger (2.10°E, 13.29°N). This paper presents the derivation of the shortwave radiation submodel. A companion article (Nicholson and Lare 1990) presents the evapoclimatonomy submodel. Lettau's third submodel, thermoclimatonomy, assumes no advective influence on surface energy balance. For the Sahel, a narrow border between the hot and hyperarid Sahara and the cool Guinea coast of the Atlantic to the South, such an assumption is invalid. Thus, the original model requires considerable reformulation. A subsequent article will describe the thermoclimatonomy parameterization and the results of the complete model simulation for wet and dry years in the Sahel. Ultimately, this model will be applied to numerical tests of the feedback hypothesis and will be compared with satellite-derived estimates of many of the parameters which it calculates.

2. Shortwave radiation climatonomy

a. Governing equations

The shortwave submodel is a solution to the energy balance equation derived by the observation or parameterization of nine dimensionless variables and the description of the physical relationships between them. The nondimensionality is a convenience achieved by dividing any energy flux by the extra-atmospheric irradiance I' (approximated as $I_0 \cos\theta$, where I_0 is the solar constant and θ is the solar zenith angle).

The nine variables include 1) five shortwave flux quantities, 2) contributions to the attenuation of beam

TABLE 1. Summary of climatonomy model characteristics (from Lettau and Lettau 1975).

Submodel	Forcing functions	Response/output
I. Shortwave radiation	Irradiance, I' (top of atmosphere)	Top or planetary albedo, A^* Absorption by submedium, $(1 - a_s)G^*$
II. Evapoclimatonomy	Precipitation, P and Absorption by submedium, $(1 - a_s)G^*$	Soil moisture, m Runoff, N Evapotranspiration, E
III. Thermal radiation	Absorption by submedium minus evapotranspiration, $(1 - a_s)G^* - E$	T_{air}, T_{sfc} Surface fluxes Net radiation, R_{net}

radiation by scatterers and absorbers, and 3) two coefficients which define the scattering process. These are summarized in Table 2. The physical relationships between these dimensionless variables yield five budget equations. The first one states that the fraction of shortwave radiation not reflected to space must equal the sum of absorption by the atmosphere H^* and by the ground $(1 - a_s)G^*$,

$$1 - A^* = H^* + (1 - a_s)G^* \quad (1)$$

where G^* is global radiation, a_s is surface albedo and A^* is top albedo. The second equation considers beam radiation $(G^* - d^*)$, or the difference between global and diffuse radiation. Its attenuation $(1 - G^* + d^*)$ must equal the depletion by scatterers σ and absorbers α, or

$$1 - G^* + d^* = \alpha + \sigma. \quad (2)$$

The third equation equates the top albedo A^*, or solar radiation reflected spaceward, with the sum of spaceward primary scattering plus ground-reflected scattering, which is neither absorbed in the air nor scattered back to the ground. Thus,

$$A^* = \mu\sigma + (1 - \alpha)a_s G^*(1 - \kappa\sigma) \quad (3)$$

using μ to denote the fraction of spaceward scattering of the solar beam and the bulk scattering coefficient κ to denote the fraction of backscatter of ground-reflected radiation (Table 2). Although this formulation does not explicitly treat multiple scattering processes, which can be significant in a dust-laden environment like the Sahel, these are implicit in the value of κ. The fourth equation expresses diffuse radiation at ground level as the sum of the downward directed primary scattering $(1 - \mu)\sigma$ and the ground-reflected radiation, which is likewise scattered downward toward the surface:

$$d^* = (1 - \mu)\sigma + (1 - \alpha)a_s G^*\kappa\sigma. \quad (4)$$

The first four equations are independent, but the fifth, which follows, is not. Assuming no net gain or loss of surface radiation locally in the long-term annual mean, the left- and right-hand sides of Eqs. (1) through (4) must balance, yielding

$$H^* = \alpha(1 + a_s G^*) \quad (5)$$

which expresses the heating function (fraction absorbed in the atmosphere) as the sum of absorption of beam radiation plus ground-reflected radiation.

With four independent equations and nine unknowns, the overall surface shortwave radiation balance can be calculated only if five variables are observed or prescribed by model assumptions. Those variables are determined by the available data and the specific application of the shortwave radiation climatonomy model.

b. *The forcing function: solar irradiance at the top of the atmosphere*

The solar irradiance at the top of the atmosphere I' is strictly a function of orbital mechanics (assuming the solar constant is invariable) and is defined to be

$$I' = I_0(\bar{d}/d)^2[(1/\pi)(H \cdot \sin\phi \cdot \sin\delta + \cos\phi \cdot \cos\delta \cdot \sin H)] \quad \text{W m}^{-2} \quad (6)$$

where I_0 is the solar constant in W m^{-2}, $(\bar{d}/d)^2$ is a measure of eccentricity (d is earth–sun distance), H is the sunrise hour angle in radians, ϕ is the latitude and δ is the solar declination. The bracketed term is the daily integrated equivalent to the cosine of the solar zenith angle θ. Following Spencer (1971), the above was calculated using a Fourier series to describe the eccentricity and solar declination as a function of the day of the year. This also allows for the calculation of H as $\cos^{-1}(-\tan\theta \cdot \tan\delta)$. The value of the solar constant is taken to be 1367 W/m^2 (Frohlich and Brusa 1981). The resulting forcing function is given in Table 3.

TABLE 2. Calculated and input variables used in the shortwave radiation submodel.

Forcing function
- $I_0 \cos\theta$ = irradiance at top of atmosphere (I')

Calculated shortwave fluxes
- A^* = top albedo of column, i.e., planetary albedo
- G^* = global radiation, or radiation received at the surface from direct and diffuse radiation
- d^* = diffuse radiation, or radiation received at the surface from the sky alone
- H^* = radiation absorbed in the atmosphere, or solar heating of the air
- a_s = surface albedo

Input necessary to define attenuation of non-dimensional beam radiation
- σ = that part of attenuation due to scattering
- α = that part of attenuation due to absorption

Coefficients that define the scattering process
- μ = fraction of effective outward scattering to space of solar beam
- κ = effective fractional amount of backward scattering of ground reflected radiation

TABLE 3. Input data used to calculate model parameters for clear skies.

Variable	Jan	Feb	Mar	Apr	May	Jun	Jul	Aug	Sep	Oct	Nov	Dec	Ann
I' (MJ m^{-2} d^{-1})	30.40	33.37	36.37	38.05	38.26	37.97	37.93	37.84	36.79	34.30	31.19	29.40	35.16
w (cm)	1.4	1.3	1.6	2.3	3.6	4.2	4.5	4.7	4.7	3.9	2.2	1.6	2.9
u (cm STP)	0.247	0.254	0.259	0.264	0.261	0.258	0.242	0.238	0.232	0.230	0.230	0.232	0.246
r (ppm)	330	330	330	330	330	330	330	330	330	330	330	330	330
β	0.37	0.31	0.63	0.69	0.69	0.51	0.51	0.44	0.36	0.45	0.40	0.33	0.47
a	0.60	0.44	0.35	0.38	0.24	0.32	0.30	0.55	0.37	0.30	0.28	0.49	0.38
M'	1.79	1.66	1.55	1.50	1.50	1.52	1.51	1.49	1.52	1.60	1.74	1.83	1.60
e (mb)	6.7	6.0	8.0	13.5	21.5	24.5	26.1	27.0	27.1	23.0	12.5	8.0	17.0

c. Absorption parameterization for clear skies

Solar radiation is absorbed primarily by water vapor (α_w), ozone (α_{o_3}), oxygen (α_{o_2}), carbon dioxide (α_{co_2}) and aerosols (α_a). The total fraction absorbed may be expressed as

$$\alpha = \alpha_w + \alpha_{o_3} + \alpha_{o_2} + \alpha_{co_2}(1 - \alpha_w) + \alpha_a. \quad (7)$$

All coefficients depend both on atmospheric composition, which is most variable for water vapor and aerosols, and on the path length of the solar beam through the atmosphere. The $\alpha_{co_2}\alpha_w$ term adjusts the absorptivity in the overlapping absorption bands of carbon dioxide and water vapor.

Path length (Rodgers 1967) is expressed with the aid of a quantity called *relative* optical air mass M calculated from solar zenith angle θ as

$$M = 35 \cdot \sec\theta \cdot (1224 + \sec^2\theta)^{-1/2} \quad (8)$$

where M has a value of 1.0 when the sun is directly overhead. Following Lunde (1980), we have applied an altitude correction, based on surface pressure, to the value of M calculated with Eq. (8). This parameter, given in Table 3, is henceforth designated as M' and referred to as the pressure-corrected optical air mass.

1) WATER VAPOR ABSORPTION

Absorption by water vapor accounts for most of the shortwave radiation absorption. We have adopted the parameterization of Lacis and Hansen (1974), which uses Yamamoto's (1962) absorption curve. The fraction of shortwave absorption by water vapor is expressed as

$$\alpha_w = 2.9M'_w/[(1 + 141.5M'_w)^{0.635} + 5.925M'_w] \quad (9)$$

where $M'_w = w'M$ is the pressure-corrected relative optical water vapor path length. The parameter w', calculated from the observed precipitable water w (Table 3) with pressure and temperature corrections (Paltridge and Platt 1976), represents the water vapor path length of a vertical column.

We have calculated monthly precipitable water at Niamey from vapor pressure data e (Table 3), using an empirical relationship derived by ben Mohamed and Frangi (1983) from sunphotometer measurements. The requisite long-term means of vapor pressure, temperature and surface pressure data were obtained from *Agroclimatological Data* (FAO 1984) and *Climates of Africa* (Griffiths 1972). Calculated monthly means of precipitable water range from 1.3 cm during the dry season to 4.7 cm during the wet season, in good agreement with measurements made by ben Mohamed and Frangi (1983) for 1981 and 1982.

2) OZONE ABSORPTION

The assessment of ozone absorption also follows Lacis and Hansen (1974). The absorption in the ultraviolet and visible regions of the spectrum are separately derived as functions of the pressure-corrected relative optical ozone path length $M'_{o_3} = uM$, where u is the actual integrated ozone amount (cm) in a vertical column. Absorptivity in the visible region is expressed as

$$\alpha_{o_3}^{vis} = 0.02118M'_{o_3}/(1 + 0.042M'_{o_3} + 0.000323M'^2_{o_3}) \quad (10)$$

while that in the ultraviolet region is given by

$$\alpha_{o_3}^{uv} = [1.082M'_{o_3}/(1 + 138.6M'_{o_3})^{0.805}] + \{0.0658M'_{o_3}/[1 + (103.6M'_{o_3})^3]\}. \quad (11)$$

Maximum error is $\leq$0.1% in the visible and $\leq$0.5% in the ultraviolet (NTP). The total fraction of incident radiation absorbed by ozone is expressed as

$$\alpha_{o_3} = \alpha_{o_3}^{uv} + \alpha_{o_3}^{vis}. \quad (12)$$

Monthly mean ozone data for Niamey (Table 3) were obtained from London et al. (1976), who analyzed ten years of measurements made with a Dobson spectrophotometer.

3) ABSORPTION BY OXYGEN AND CARBON DIOXIDE

Absorption of solar radiation by oxygen and carbon dioxide is relatively minor in comparison with that by water vapor and ozone. Following Sasamori et al. (1972), we have calculated oxygen absorptivity as

$$\alpha_{o_2} = 7.5 \times 10^{-3}(M')^{0.875} \quad (13)$$

where M' is the altitude- (i.e., pressure-) corrected optical air mass. That for carbon dioxide is calculated as

$$\alpha_{co_2} = 2.35 \times 10^{-3}(M'_{co_2} + 0.0129)^{0.26} - 7.5 \times 10^{-4} \quad (14)$$

where M'_{co_2} is the pressure-corrected path length of carbon dioxide (cm), which can be calculated (Redmond 1980) from carbon dioxide concentration r (Table 3).

4) AEROSOLS

The basic equation to describe aerosol attenuation is that of Ångström:

$$\delta_a(\lambda) = \beta\lambda^{-a} \quad (15)$$

which relates the aerosol optical depth δ_a at wavelength λ to a turbidity coefficient β and a wavelength exponent a. Application of this equation to total atmospheric aerosol absorption α_a, the parameter required in the climatonomy model, is complex and a number of alternative approaches have been derived. Aerosol absorptivity is defined as

$$\alpha_a = (1 - \tilde{w})(1 - \gamma_a) \quad (16)$$

where γ_a is the aerosol transmissivity and $\tilde{w}$ is the aerosol single scattering albedo. The latter represents the ratio of the aerosol scattering optical depth to the total aerosol optical depth δ_a. Thus, an assessment of α_a requires only two parameters: the aerosol transmissivity and the single scattering albedo for Saharan aerosols. Observations during the ECLATS experiment show that the latter ranges from about 0.94 to 0.96, which agrees well with Mie theory calculations based on Saharan aerosol characteristics (Cerf et al. 1982; Fouquart et al. 1987). A value of 0.95 is used in our model.

A number of studies have assessed turbidity over West Africa and have produced data from which aerosol transmissivity can be estimated. For the most part, these consist of ground-based sunphotometer measurements from which values of the Ångström turbidity coefficient β and wavelength exponent a have been calculated and published. These indirectly provide γ_a, by application of two empirical formulas, which relate both γ_a and β to horizontal visibility VV. The first, developed by Mächler (1983) (see Iqbal 1983; p. 177) through a regression analysis of transmissivity via Ångström's turbidity equation, gives transmissivity as

$$\gamma_a = [0.97 - 1.265(VV)^{-0.66}]^{(M'^{0.9})} \quad (17)$$

where M' is actual (i.e., pressure-corrected) optical air mass. The second, from d'Almeida (1986), relates visibility to β, based on data for several West African stations:

$$VV = (\beta/2.26)^{-1.37}. \quad (18)$$

These approximations are most likely to be valid if water vapor content is relatively low and aerosols are distributed throughout much of the atmospheric column. In the Sahel, this is the case during the months of high dust concentration.

Actual visibility data, although preferable, were not readily available but β has been assessed for a number of West African locations. We have used two sources of measurements at Niamey: Cerf's (1980) data for the years 1976 and 1978/79 and ben Mohamed and Frangi's (1986) data for the years 1981 and 1982. These measurements were averaged to produce the monthly β values of Table 3, which we used to assess transmissivity from Eqs. (17) and (18), and subsequently aerosol absorptivity from Eq. (16). The absorption by aerosols is approximately 10% of the total absorption of shortwave radiation and is roughly comparable to the combined contribution of carbon dioxide and oxygen.

The values of the turbidity coefficient (Table 3) range from 0.31 early in the dry season to 0.69 just prior to the rainy season when they drop sharply. The maximum values of β (i.e., the dustiest conditions) occur in March to May. The minimum occurs during August through February, but with considerable variation from month to month. Since the dataset consists of only 28 months of observations, this variability may be due to a handful of random dust outbreaks. Presumably, a larger period of record would produce a smoother curve. These values are nonetheless in close agreement with measurements made at other Sahelian stations, such as Gao, Boutilimit, Dakar, Ouagadougou and Agadez (Holben, personal communication; Cerf 1980; d'Almeida 1986). Agadez, however, which is furthest north, has somewhat higher values and a later maximum, presumably because the onset of the rainy season is later than at more southern stations.

It must be realized that the years for which measurements were available, from the mid-1970s to early 1980s, were those of relatively low rainfall and probably high aerosol content (Nicholson 1985; Prospero and Nees 1986). Visibility data obtained for three anomalously wet years in the 1950's show that atmospheric turbidity, i.e., aerosol concentration, was significantly lower than the data from the 1970s and 1980s indicate. Thus, long-term means of β and aerosol absorptivity are probably somewhat lower than those in Table 3.

d. Scattering parameterization for clear skies

For clear skies only two scattering processes are of consequence: Rayleigh (molecular) and aerosol scattering. Thus, the total scattering σ can be expressed as

$$\sigma = \sigma_R + \sigma_a \quad (19)$$

where σ_R and σ_a, respectively, denote the Rayleigh and aerosol contributions to the process. For Rayleigh scattering, σ_R, we have chosen the parameterization developed by Bird and Hulstrom (1981):

$$\sigma_R = 1 - \exp[-0.0903M'^{0.84}(1.0 + M' + M'^{1.01})] \quad (20)$$

where M' is the actual pressure-corrected optical air mass. Precise aerosol scattering parameterization is more complex and requires considerable information about the nature and quantity of particulate loading. The single scattering albedo for Saharan dust is assumed to be 0.95 (section 2c). Since the single scattering albedo approximately represents the portion of beam attenuation that can be attributed to scattering, we can infer that, to a first approximation,

$$\sigma_a \approx 19\alpha_a. \quad (21)$$

This is consistent with the findings of Fouquart et al. (1987) that Saharan dust is predominantly a scatterer of shortwave radiation and an absorber of longwave.

To assess the impact of atmospheric scattering on surface energy balance, two additional parameters are needed: μ, the fraction of effective outward scattering to space, and κ, the effective fraction of backscatter of ground-reflected solar radiation. A series of monthly values of μ (Table 4) was derived from

$$\mu = 1 - F_c \quad (22)$$

where F_c is the ratio of downward to upward scattering as given by Robinson (1962) and Iqbal (1983). The F_c is a function of the relative optical air mass M. The values we determined for Niamey are less than the value of ⅓ tentatively assigned to μ by Lettau and Lettau (1969). For κ, these authors have suggested unity for very dry locations and 0.75 for prairie conditions (comparable to the wet season in Niamey). Here, we have set κ to unity during January through March then decreasing to 0.75 for July through September (Table 4).

e. Surface albedo

Long-term albedo measurements for Niamey do not exist and a wide range of values for similar savanna landscapes in Africa has been published. Several sources were evaluated to derive a representative set of monthly surface albedos for the area. Some of the notable satellite observations are those of Rockwood and Cox (1978), who found dry season values of 0.26 to 0.31 for the savanna of northwestern Africa and 0.21 to 0.26 for the wet season, and those of Norton et al. (1979), whose limited reported measurements (one or two per year) indicate a range of 0.24 to 0.33 for the Niamey region. Albedo does, however, exhibit significant interannual variability, primarily in response to rainfall and vegetation changes (Norton et al. 1979; Courel et al. 1984); a minimum observed by satellite is about 0.20.

These generally agree with figures published by Oguntoyinbo (1970) and Sellers (1965) for savanna vegetation. The area surrounding Niamey is typified by widely spaced acacia trees and perennial grasses near 80 cm in height (Cochemé and Franquin 1967). This region is a borderland between the Sudanese savanna and the more arid Sahel, and ground-based measurements for such regions are generally 0.25 to 0.30 for the dry season and 0.15 to 0.20 for the wet season. Considering the conventional data based on vegetation types, satellite observations for the region specifically, the seasonal cycle of rainfall, and the periods of green-up and senescence of vegetation, we have chosen the monthly albedo values given in Table 4 for surface energy balance calculations. A minimum value of 0.20 is assigned to August and September, a maximum of 0.30–0.32 for January to June, after which time a rapid green-up occurs.

f. Input parameters for clear sky model

Table 4 presents the input data for the clear sky case: the model's forcing function, extra-atmospheric irradiance; the five basic input parameters of the model (the two directional coefficients of scattering μ and κ, the total scattering and absorption σ and α, and surface albedo a_s); and the partial absorption and scattering

TABLE 4. Input model parameters for clear skies case.

Parameter	Jan	Feb	Mar	Apr	May	Jun	Jul	Aug	Sep	Oct	Nov	Dec	Ann
I'	30.40	33.37	36.37	38.05	38.26	37.97	37.93	37.84	36.79	34.30	31.19	29.40	35.16
a_s	0.300	0.300	0.310	0.310	0.320	0.300	0.230	0.200	0.200	0.220	0.260	0.280	0.270
μ	0.190	0.170	0.150	0.140	0.140	0.140	0.140	0.140	0.140	0.160	0.180	0.200	0.160
κ	1.000	1.000	1.000	0.950	0.900	0.850	0.750	0.750	0.750	0.800	0.900	0.950	0.880
α_w	0.126	0.121	0.124	0.137	0.154	0.161	0.164	0.165	0.166	0.160	0.141	0.131	0.146
α_{o_3}	0.025	0.024	0.024	0.023	0.023	0.023	0.023	0.023	0.022	0.023	0.024	0.024	0.024
α_{o_2}	0.012	0.011	0.010	0.010	0.010	0.010	0.010	0.010	0.010	0.011	0.012	0.012	0.011
α_{co_2}	0.008	0.008	0.008	0.007	0.007	0.007	0.007	0.007	0.007	0.007	0.008	0.008	0.007
α_a	0.020	0.017	0.027	0.029	0.029	0.023	0.023	0.020	0.018	0.022	0.021	0.019	0.022
α	0.191	0.181	0.193	0.206	0.223	0.224	0.227	0.225	0.223	0.222	0.205	0.194	0.210
σ_R	0.130	0.123	0.116	0.113	0.114	0.115	0.114	0.113	0.115	0.120	0.127	0.133	0.119
σ_a	0.385	0.320	0.517	0.543	0.544	0.437	0.436	0.387	0.336	0.413	0.400	0.361	0.423
σ	0.515	0.443	0.633	0.656	0.658	0.552	0.550	0.501	0.451	0.532	0.527	0.493	0.543

coefficients for the various atmospheric constituents. The beam attenuation is clearly dominated by the scattering process. Total scattering depletes the solar beam by just over 50% in the annual average, but most of the scattered portion still reaches the ground as diffuse radiation. Absorption further attenuates solar radiation by about 21%, with little monthly variation.

A high concentration of atmospheric dust is an inherent feature of the Sahelian climate. The data in Table 4 suggest that its contribution to the scattering process is nearly four times greater than that of molecular Rayleigh scattering. Turbidity and the associated attenuation increase abruptly in March when the winds pick up, vegetation dies off and the ground dries up, thus promoting dust production. The aerosol effect drops in June, when the rains become frequent and vegetation growth begins. It remains low throughout the rainy season and well into the dry season. Total aerosol scattering ranges from 32% in February to 54% in April and May, compared to a maximum contribution to atmospheric absorption of 3%. The monthly variation of total scattering parallels that by aerosols, reaching 66% in May and falling to 44% in February.

The largest contribution to absorption is by water vapor; monthly values range from 12% to 17% of the incoming solar beam (Table 4). Ozone and aerosols each absorb between 2% and 3% of the incoming radiation, while oxygen and carbon dioxide combined absorb less than 2%. Because water vapor makes both the largest and most variable contribution, total absorption closely parallels the seasonal cycle of precipitable water and thus has a maximum during the rainy season from May through October. The absorption by other gaseous constituents and aerosols is only about 30% of the total atmospheric absorption of solar radiation.

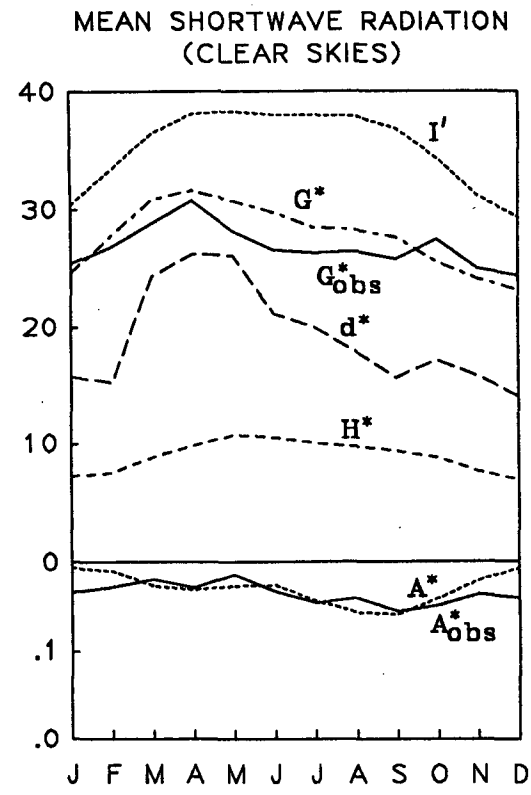

FIG. 1. Monthly means of shortwave radiation components (global radiation G^*, diffuse radiation d^*, atmospheric heating H^* and planetary albedo A^*) for clear skies as calculated by the shortwave radiation submodel. Observed values of planetary albedo A^*_{obs} and global radiation G^*_{obs} and the forcing function I' (irradiance at the top of the atmosphere) are included for comparison. Units are MJ m^{-2} day^{-1} except for planetary albedo, which is expressed as a fraction of the forcing function I'. Note that the dimensionless variables have been multiplied by the forcing function I', to obtain the indicated units. This is true of all subsequent figures.

g. Results for clear skies

In the present study the primary model output consists of global radiation reaching the surface G^*, total atmospheric absorption H^*, diffuse radiation d^* and top albedo A^* (Fig. 1, Table 5). Global radiation, like extra-atmospheric irradiance, peaks from March to August, but within this period, it shows a gradual decline from April on as atmospheric humidity and later turbidity increase. Diffuse radiation peaks in March, April and May, when the aerosol content is at a maximum. It generally totals about ½ to ⅔ of the global radiation. Planetary albedo attains a maximum of 0.19 from December to February and a minimum of 0.14 during the rainy season months of August and September.

Verification of model results is somewhat problematic because the appropriate comparison is with observed values on cloud-free days. Such information is, however, rarely available and published radiation balance data are for "mean" conditions, i.e., the partly cloudy case modeled in section 3. We have attempted to approximate the observations for cloud-free days with maximum daily values of global radiation and minimum planetary albedo.

The former were provided by Dr. M. V. K. Sivakumar of the International Crops Research Institute for the Semi-Arid Tropics (ICRISAT) in Niamey and were available for the years 1983 to 1987. Figure 1 shows the maximum observed daily value of global radiation for each month, which presumably approximates clear sky radiation if the month has at least one cloud-free day within the 5-year period. The differences between these values and model estimates of clear sky global radiation are about 3%–5% during the dry season, when the model estimates are generally lower than the observed. The difference is 7%–9% during all wet season months except June, when it is nearly 12%. The model estimates are consistently higher than the maximum daily values during the wet season, presumably because the assumption of at least one cloud-free day is unlikely: mean cloudiness is 70%–80% in most months.

TABLE 5. Monthly mean shortwave radiation results for Niamey, Niger under clear skies. Irradiance at the top of the atmosphere I', atmospheric heating H^*, direct beam radiation D^*, diffuse radiation d^* global radiation G^* and absorbed solar radiation by the ground $(1 - a_s)G^*$ have units of MJ m^{-2} day^{-1}. Planetary albedo A^* is a fraction of the irradiance at the top of the atmosphere for the prescribed surface albedo a_s, absorptivity α (α_g is that by carbon dioxide and oxygen) and scattering σ.

	Jan	Feb	Mar	Apr	May	Jun	Jul	Aug	Sep	Oct	Nov	Dec	Ann
I'	30.4	33.4	36.4	38.0	38.3	38.0	37.9	37.8	36.8	34.3	31.2	29.4	35.2
a_s	.300	.300	.310	.310	.320	.300	.230	.200	.200	.220	.260	.280	.269
σ_R	.130	.123	.116	.113	.114	.115	.114	.113	.115	.120	.127	.133	.119
σ_a	.385	.320	.517	.543	.544	.437	.436	.387	.336	.413	.400	.361	.423
σ	.515	.443	.633	.656	.658	.552	.550	.501	.451	.532	.527	.493	.543
α_w	.126	.121	.124	.137	.154	.160	.163	.165	.165	.160	.140	.131	.146
α_{o_3}	.025	.024	.024	.023	.023	.023	.023	.023	.022	.023	.024	.024	.023
α_g	.020	.019	.018	.018	.018	.018	.018	.017	.018	.018	.019	.020	.018
α_a	.020	.017	.027	.029	.029	.023	.023	.020	.018	.022	.021	.019	.022
α	.191	.181	.193	.206	.223	.224	.227	.225	.223	.222	.205	.194	.210
H^*	7.2	7.5	8.9	9.9	10.7	10.5	10.1	9.8	9.4	8.9	7.7	7.0	8.9
D^*	8.9	12.5	6.3	5.2	4.5	8.5	8.5	10.4	12.0	8.4	8.4	9.2	8.7
d^*	15.8	15.3	24.5	26.3	26.2	21.3	20.0	17.9	15.7	17.2	15.9	14.1	18.8
G^*	24.7	27.9	30.8	31.5	30.7	29.8	28.5	28.3	27.7	25.6	24.2	23.2	27.5
$(1 - a_s)G^*$	17.3	19.5	21.2	21.8	20.9	20.8	21.9	22.7	22.2	20.0	17.9	16.7	20.1
A^*	.194	.190	.173	.169	.173	.174	.156	.143	.141	.159	.179	.193	.174

Minimum planetary albedo values were obtained from B.-J. Sohn (Florida State University), whose analysis used Nimbus 7 ERB data in conjunction with NOAA 6 and 7 and Tiros N data for the period January 1979, to December 1983. Data were gridded on 2.5° squares. Figure 1 shows the minimum albedo for each month during the five-year period for the square surrounding Niamey, which was centered at 2.5°E and 12.5°N. These values are exceedingly close to model calculations except for December and January, when the observed are about 12% lower than calculated. An examination of ancillary data for these months suggests that this is not a systematic model error but a result of exceedingly high rainfall in 1980 and 1981. The model simulates *mean* clear sky conditions; minimum albedo would represent such conditions if 1) at least one cloud-free day is available for each month and 2) model input parameters show little interannual variability. This is not true for surface albedo, since vegetation cover changes markedly from year to year. In fact, the December and January values of minimum albedo in Fig. 1 correspond to months of anomalously high vegetation growth (Malo 1988), a consequence of the high rainfall in 1980 and 1981, and therefore anomalously low surface albedo.

3. Shortwave radiation submodel for partly cloudy skies

a. *Basic model equations*

The climatonomy model uses a stark simplification of cloud processes so that the results are applicable only for gross, large scale effects (Lettau and Lettau 1969). A basic assumption is that for partly cloudy skies, the contributions of cloudy and clear air to the absorption process are additive, while contributions to scattering are distributive, i.e., must be prorated. This assumption is expressed as

$$\alpha = (1 - c)\alpha_0 + c(\alpha_0 + \alpha_c) = \alpha_0 + c\alpha_c \quad (23)$$

$$\sigma = (1 - c)\sigma_0 + c\sigma_c = \sigma_0 + c(\sigma_c - \sigma_0) \quad (24)$$

where c is cloudiness (percent) and the subscripts 0 and c relate to clear and cloudy air, respectively.

The basic climatonomic equations may be so modified. Then, the top albedo is the sum of a prorated contribution from the clear area plus direct reflection from the cloud-covered portions. Hence,

$$A^* = (1 - c)A_0 + c[A_c + a_sG^*(1 - \alpha)(1 - A_c)] \quad (25)$$

where A_0 is planetary albedo for clear skies, A_c is an "effective" cloud albedo calculated as $A_c = \mu_c\sigma_c$, and the portion scattered earthward by the cloud is $(1 - \mu_c)\sigma_c$. The fraction μ_c is analogous to μ for clear skies and represents the ratio of spaceward scattering to total scattering of beam radiation by the cloud. The corresponding equation for atmospheric heating in the case of partly cloudy skies is

$$H^* = (1 - c)H_0^* + c\alpha(1 + a_sG^*) \quad (26)$$

where the right-most term represents absorption of the direct beam plus solar radiation reflected from the surface. The final equation is the sum of (25) and (26) and, when solved for G^*, becomes

$$G^* = [1 - A_0 - H_0^* + c(A_0 + H_0^* - A_c - \alpha)]/[1 - a_s + ca_s(1 - A_c + \alpha A_c)] \quad (27)$$

which corresponds to Eqs. (3) and (5) for clear skies.

b. Input data for mean conditions of cloudiness

Four bulk cloud parameters must be determined for a climatonomic description of the energy balance for partly cloudy skies: α_c, A_c, μ_c, and σ_c. These all depend greatly on the characteristics of individual clouds and on atmospheric turbidity. A wide range of values of cloud albedo and absorptivity has been published, but less information is available for the other two parameters. For individual cloud types, the model uses the albedos and absorptivities in Table 6, based principally on Liou (1976) and Drummond and Hickey (1971). Absorptivity ranges from 0 for cirroform clouds to 0.19 for cumulonimbus and nimbostratus. Albedo ranges from 0.20 for cirroform to 0.78 for the nimbus types.

Using the values in Table 6, mean seasonal bulk absorptivity α_c and albedo A_c are calculated as in Warren et al. (1986), prorating the contribution of individual cloud types according to the formula

$$\alpha_c(k) = \left[\frac{\sum_{i=1}^{N} (f_{k,i})(\mathrm{amt}_{k,i})(\alpha'_i)}{\sum_{i=1}^{N} (f_{k,i})(\mathrm{amt}_{k,i})}\right] \quad \text{where}$$

$$k = 1, 2, 3, 4 \text{ season} \quad (28)$$

for absorption and an analogous formula for cloud albedo A_c. In the above, k denotes the season, i denotes the cloud type, and N denotes the total number of cloud types which can be discriminated from available data. Then, $f(k, i)$ and $\mathrm{amt}(k, i)$, respectively, denote the seasonal frequency and amount of cloud type i during season k, and α'_i denotes the absorptivity of cloud type i. When A_c is calculated, α'_i in Eq. (28) is replaced by A'_i, the albedo corresponding to individual cloud types. The cloud data for Niamey which were used in these calculations were derived from Warren et al. (1986), who discriminate six classes of clouds (Table 6).

These seasonal values were then used to extrapolate monthly values of α_c and A_c, given in Table 7. Mean monthly cloud cover (Table 7) was also obtained from Warren et al. (1986), whose study was based on a few recent years, which have been quite dry. To assure that these data are reasonably representative of long-term mean conditions, we have compared them with data in Griffiths (1972) and with data from the 1950s (a wet period) obtained from the Meteorological Service of Niger. There was very good agreement.

The remaining two parameters μ_c and σ_c, the directional coefficient of scattering and bulk cloud scattering were roughly estimated on the assumption that μ_c is primarily a function of cloud thickness. Based on this assumption and the values of μ' given in Lettau and Lettau (1969), μ' has been estimated for individual cloud types and used to calculate σ' from A' (Table 6). Monthly series of σ_c were then derived in the same manner as α_c and A_c (Table 7), using Eq. (28). These calculations were also subject to the constraint that absorption plus scattering cannot exceed unity. This imposed an upper limit to σ_c and σ'. The case that α' plus σ' equals unity implies that only diffuse radiation is ultimately transmitted. This occurred only with cumulonimbus and nimbostratus, which frequently totally deplete direct beam radiation.

Tables 7 and 8 present the bulk model input parameters for partly cloudy skies. Cloudiness, which ranges from 45% in January to 78% in August, has its greatest effect on scattering. It tends to scatter about 30%–60% of the solar beam but absorb less than 6%. Scattering and absorption increase dramatically during the rainy season (mainly July and August), when cumulonimbus clouds are often present and total cloudiness is at a maximum. Throughout the year clouds are the dominant factor in scattering, but cloud absorption is comparable to that of the dry gaseous constituents and about one-third that of water vapor. Compared to clear

TABLE 6. Input data for cloud portion of model.

a) Frequency and amount (in percent) of various cloud types by season

	Cu		Cb		St, Sc, Fog		Ns		At, As		Ci, Cs, Cc	
	Freq	Amt	Freq	Amt	Freq	Amt	Freq	Amt	Freq	Amt	Freq	Amt
DJF	1	24	1	17	1	22	0	0	14	39	85	56
MAM	10	25	9	30	5	30	0	93	36	49	93	65
JJA	13	32	21	35	22	46	1	98	65	60	91	60
SON	9	27	14	33	9	39	1	94	39	49	90	58

b) Scattering coefficient (σ'), fraction of upward scattering (μ'), absorptivity (α') and cloud albedo (A') by cloud type

	Cu	Cb	St, Sc, Fog	Ns	At, As	Ci, Cs, Cc
σ'	.73	.81	.77	.81	.80	.67
μ'	.77	.96	.73	.96	.70	.30
α'	.075	.19	.075	.19	.15	.00
A'	.56	.78	.56	.78	.56	.20

TABLE 7. Bulk parameterization for cloud portion of model.

Variable	Jan	Feb	Mar	Apr	May	Jun	Jul	Aug	Sep	Oct	Nov	Dec	Ann
c (%)	45	49	61	68	73	70	76	78	71	63	50	51	63
σ_c	0.680	0.680	0.700	0.710	0.720	0.725	0.730	0.735	0.730	0.720	0.710	0.680	0.710
μ_c	0.350	0.370	0.390	0.440	0.490	0.540	0.560	0.590	0.530	0.500	0.420	0.340	0.460
α_c	0.016	0.018	0.030	0.040	0.056	0.070	0.073	0.076	0.060	0.045	0.027	0.014	0.044
A_c	0.240	0.250	0.270	0.310	0.350	0.390	0.410	0.430	0.390	0.360	0.300	0.230	0.330

skies, scattering is generally increased by the presence of clouds, but only marginally so in the months of greatest turbidity, March to May. The months of maximum and minimum scattering and absorption are generally the same in both the clear sky and partly cloudy cases.

c. *Model results for partly cloudy skies*

The most notable differences between the clear sky (Fig. 1) and partly cloudy cases (Fig. 2) are the magnitude and seasonality of global radiation and the contribution of diffuse radiation to the global. The model for partly cloudy skies shows a pronounced decrease of both global and diffuse radiation during the wet season, with minima in August. The ratio of global radiation under mean conditions of cloudiness to that with clear skies varies from 53% in August to 86% in December and January (Fig. 3). The diffuse portion totals at least 80% of the radiation received at the surface in all months, compared to generally 50% to 80% in the clear sky case. From May to August, however, the diffuse contribution comprises nearly all of the global radiation. This result seems reasonable in view of the high atmospheric dust loading and the high cloud cover (70 to 80%) during these months, and the high aerosol content of the clouds. Aerosol-laden clouds have a high optical thickness and a high single scattering albedo, which increases reflection and reduces transmission (Twomey 1978).

For model verification, we have obtained mean global radiation from *Agroclimatological Data* (FAO 1984), based on ten or more recent years, and mean planetary albedo from Smith and Smith (1987) for the period 1979–1983. The observed values (Fig. 2) show that planetary albedo and global radiation are both fairly steady throughout the year; the latter has slight minima in December (when solar irradiance is low) and August (when cloudiness peaks). The seasonal variation in the model calculations is considerably larger. Thus, the model tends to overestimate planetary albedo during the wet season and underestimate it during the dry season by 10%–15%. Consistent with this, the model underestimates global radiation during the wet season and overestimates it during the dry season. The error is generally 0%–15%, except for July and August, months when mean cloudiness approaches 80%.

The sensitivity studies described in section 4 suggest that the discrepancies between model estimates and observed parameters can best be accounted for by the

TABLE 8. Monthly mean shortwave radiation results for Niamey, Niger under partly cloudy skies. Irradiance at the top of the atmosphere I', atmospheric heating H^*, direct beam radiation D^*, diffuse radiation d^*, global radiation G^* and absorbed solar radiation by the ground $(1 - a_s)G^*$ have units of MJ m^{-2} day^{-1}. Planetary albedo A^* is a fraction of the irradiance at the top of the atmosphere for the prescribed surface albedo a_s, absorptivity α (α_g is that by carbon dioxide and oxygen) and scattering σ.

	Jan	Feb	Mar	Apr	May	Jun	Jul	Aug	Sep	Oct	Nov	Dec	Ann
I'	30.4	33.4	36.4	38.0	38.3	38.0	37.9	37.8	36.8	34.3	31.2	29.4	35.2
a_s	.300	.300	.310	.310	.320	.300	.230	.200	.200	.220	.260	.280	.269
σ_R	.072	.063	.045	.037	.031	.034	.027	.026	.033	.045	.064	.065	.045
σ_a	.212	.164	.200	.176	.150	.131	.104	.087	.097	.155	.200	.176	.159
σ_c	.306	.332	.429	.479	.522	.508	.557	.570	.520	.450	.355	.348	.448
σ	.589	.559	.674	.692	.703	.673	.687	.682	.650	.650	.619	.589	.647
α_w	.126	.121	.124	.137	.154	.160	.163	.165	.165	.160	.140	.131	.146
α_{o_3}	.025	.024	.024	.023	.023	.023	.023	.023	.022	.023	.024	.024	.023
α_g	.020	.019	.018	.018	.018	.018	.018	.017	.018	.018	.019	.020	.018
α_a	.020	.017	.027	.029	.029	.023	.023	.020	.018	.022	.021	.019	.022
α_c	.007	.009	.018	.027	.041	.049	.056	.059	.043	.028	.014	.007	.027
α	.198	.190	.212	.233	.264	.273	.282	.284	.266	.251	.218	.201	.239
H^*	7.3	7.6	9.1	10.3	11.5	11.5	11.3	11.2	10.3	9.3	7.8	7.0	9.4
D^*	3.6	4.3	1.6	.9	.3	.6	.3	.3	.9	1.3	2.5	3.0	1.5
d^*	17.7	19.1	21.9	21.2	19.0	17.3	15.5	14.6	16.2	16.7	17.1	17.0	18.4
G^*	21.3	23.4	23.6	22.1	19.3	17.9	15.8	14.9	17.1	18.0	19.6	20.0	19.9
$(1 - a_s)G^*$	14.9	16.4	16.3	15.3	13.1	12.5	12.2	11.9	13.7	14.0	14.5	14.4	14.5
A^*	.272	.281	.303	.328	.357	.369	.380	.390	.348	.319	.284	.272	.319

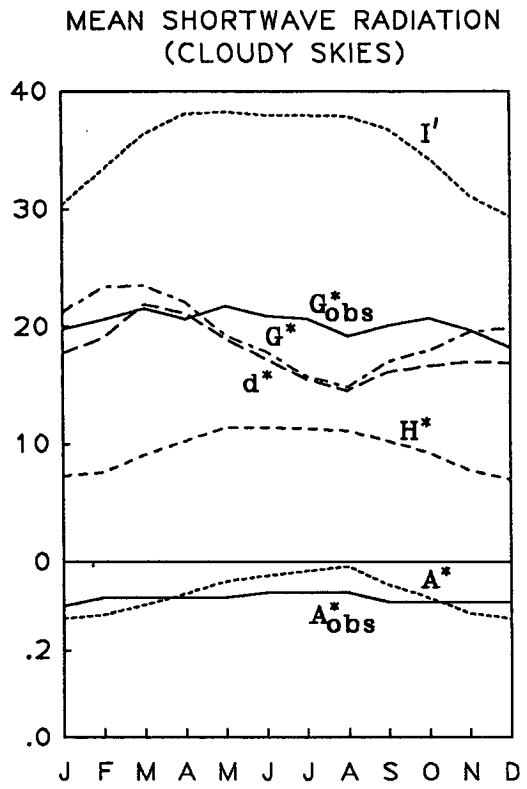

FIG. 2. As in Fig. 1, but for partly cloudy skies.

values of cloud albedo used in the model. It should be noted that the calculated difference in global radiation for clear skies and partly cloudy conditions is very close to that observed in most months (Fig. 3). The latter is estimated as the ratio between mean global radiation (Fig. 2) and the maximum daily values (Fig. 1) which we have used in section 2g to approximate the clear sky case. The model significantly underestimates the difference from May to September wet season, the period when monthly cloudiness exceeds 70%. Although this may partially reflect underestimates of observed G_0^* (clear sky case) during the wet season, it also suggests that discrepancies between the model and observations are partly due to errors in assumed values of cloud albedo during the wet season. A reduction of cloud albedos by 20% during the five wet season months brings the model error down to a few percent.

4. Sensitivity studies

We have carried out a variety of sensitivity studies by systematically modifying model parameters and evaluating the effect on global radiation G^*, diffuse radiation d^*, and planetary albedo A^* for both the clear sky and partly cloudy cases. For most variables in the shortwave submodel, the error in estimating mean monthly values is unlikely to exceed ±20%; this is also roughly the largest range of interannual variability that might be expected. Thus submodel parameters were systematically varied by ±20%. The results of these sensitivity studies are briefly summarized in this section. Changes corresponding to the expected interannual variability of Sahel climate (e.g., cloudiness, cloud albedo, surface albedo and aerosols) are illustrated in greater detail.

Sensitivity tests were conducted for the four most variable atmospheric constituents: ozone, carbon dioxide, water vapor and aerosols. Of these, the model shows the greatest sensitivity to water vapor while the others have little effect on the output variables, global radiation and planetary albedo. A 20% change in water vapor pressure generally changes these variables by less than 1.5%. The exception is the case of partly cloudy skies, where a 20% change of vapor pressure modifies some monthly means of global radiation by up to 3%. The other constituents generally change model output by considerably less than 1%.

The case of aerosols (Fig. 4a) deserves special consideration because atmospheric turbidity changes markedly from year to year, in response to rainfall fluctuations. Although large changes of aerosol concentration have little impact on global radiation, they significantly alter the ratio of diffuse to direct. The directional scattering coefficients μ and κ, which are determined primarily by the amount and nature of the aerosols and were only roughly approximated, likewise have little impact on the model unless changed by

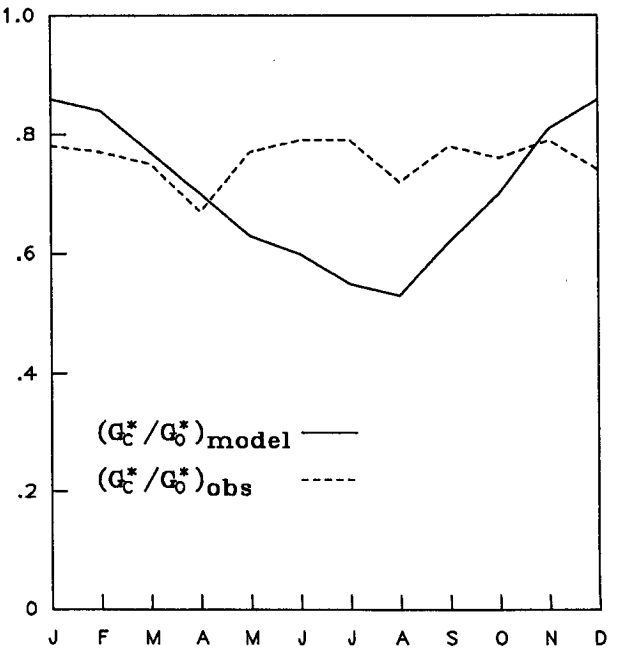

FIG. 3. Ratio of global radiation for partly cloudy skies to that under clear skies as calculated by the model (solid line) and as observed (dashed line).

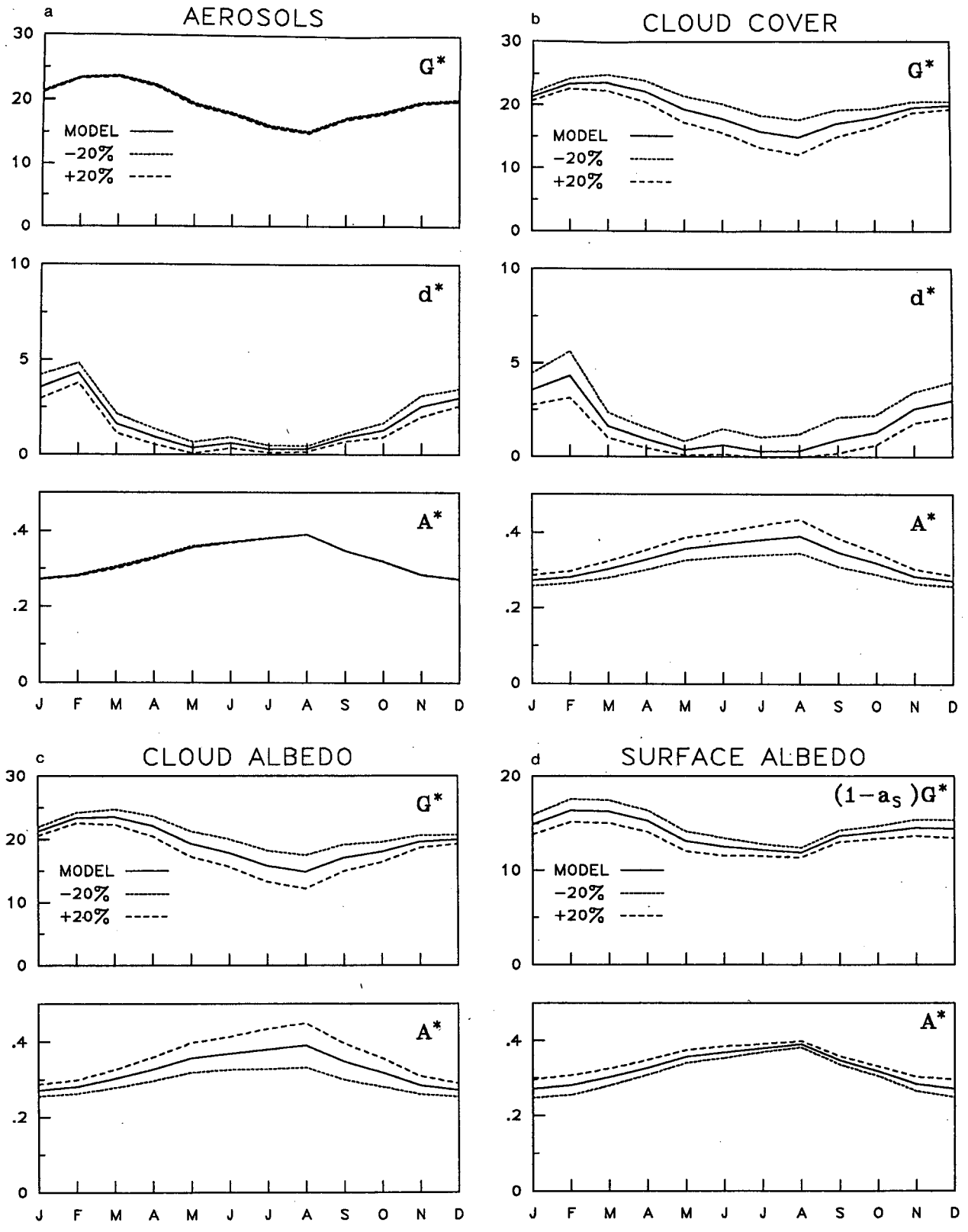

FIG. 4. (a) Effect of varying aerosol concentration by ±20% on global radiation G^*, diffuse radiation d^* and planetary albedo A^* for partly cloudy skies (units for G^* and d^*: MJ m^{-2} day^{-1}). (b) Effect of varying cloud cover by ±20% on global radiation G^*, diffuse radiation d^* and planetary albedo A^* for partly cloudy skies (units for G^* and d^*: MJ m^{-2} day^{-1}). (c) Effect of varying cloud albedo by ±20% on global radiation G^* and planetary albedo A^* for partly cloudy skies (units for G^*: MJ m^{-2} day^{-1}). (d) Effect of varying surface albedo by ±20% on ground-absorbed solar radiation $(1 - a_s)G^*$ and planetary albedo A^* for partly cloudy skies (units for $(1 - a_s)G^*$: MJ m^{-2} day^{-1}).

about 50%. In that case, monthly means of global radiation and planetary albedo are modified by up to 10% for clear skies but only 4% in the more common case of partly cloudy skies. The model is more sensitive to single scattering albedo $\tilde{w}$. Although an extensive series of recent measurements showed this to range only between $\approx$0.94 and 0.96 (Fouquart et al. 1987), an earlier study by Carlson and Benjamin (1980) found values as low as 0.86, indicating some interannual variability as the dust composition changes. This lower value would decrease calculated values of global radiation by 5%–12%.

Tests of cloud parameters show the model to be considerably more sensitive to percent cover and cloud albedo than to cloud absorptivity (Figs. 4b and 4c). Changes of cover and albedo of ±20% change global radiation by 3%–9% in the dry season and approximately 10%–19% during the wet season. The high sensitivity to clouds, though not unexpected, is significant since cloud albedo can be only roughly estimated. A wide range of values has been published and these are greatly influenced by specific cloud characteristics, which are unavailable for the Sahel.

A reduction of total cloudiness or cloud albedo of $\approx$20% results in global radiation and planetary albedo values for the wet season which are remarkably close to observed values, but accentuates the model errors in the dry season. This suggests that the errors in cloud parameterization are principally for cloud types that are most prevalent during the rainy season, e.g., cumulonimbus and low and midlevel stratoform clouds. The effect of multiple cloud layers, which are prevalent during the wet season and not handled by the model, could also account for some of the error in the model calculations.

As is the case with cloud cover, surface albedo (Fig. 4d) has a relatively large effect on the shortwave radiation budget (Fig. 1). A 20% increase in surface albedo decreases global radiation by $\approx$4%–6% under clear skies and $\approx$4%–8% with partly cloudy skies. The higher albedo enhances total backscatter of the surface-reflected radiation.

5. Summary and conclusions

The model shows that under clear sky conditions in the Sahel, the shortwave balance is determined primarily by water vapor, aerosols and surface albedo. In the annual average, 54% of the solar beam is scattered (nearly all by aerosols), but most reaches the ground as diffuse radiation. Some 21% of the solar beam is absorbed in the atmosphere: water vapor absorbs 15%; other gaseous constituents, 4%; and aerosols, 2%.

Under conditions of mean cloudiness, total beam absorption is only slightly larger (24%) but in the annual average 65% of incoming solar is scattered. Cloud scattering is about three times as great as aerosol scattering.

The model results are most sensitive to cloud amount and cloud albedo. A 20% change in either parameter also modifies global radiation at the surface by $\approx$20% during the periods of greatest cloud cover (the rainy season), but the effect on planetary albedo is considerably smaller. A 20% change in aerosol content has no effect on global radiation or planetary albedo, but does alter the ratio of diffuse to direct beam. Under conditions of mean cloudiness, a 20% change in surface albedo alters planetary albedo and absorbed solar radiation by generally less than 5% or 10%; the model results are most sensitive to surface albedo during the dry season, when cloudiness is relatively low.

For clear skies, model results are in excellent agreement with minimum planetary albedo values obtained from satellites, and in good agreement with estimates of clear-sky global radiation, based on maximum daily values of measured global radiation. In these cases, we feel that the discrepancies between model results and observations more likely reflect shortcomings of the observations available for comparison than inadequacies of the model. For example, the model estimates long-term mean conditions, but observations are generally based on a few recent years. Moreover, the observations represent *minimum* values of planetary albedo A* and *maximum* values of global radiation G^*; these are merely approximations of the parameters being modeled, *mean* values of A^* and G^* under clear skies.

The model results for mean conditions of cloudiness show greater differences from observed values of A^* and G^*. The model tends to overestimate A^* during the wet season and underestimate it during the dry season by 10%–15%. Errors in estimating G^* are about the same except for the months of July and August, when mean cloudiness approaches 80%. Then the discrepancy between calculated and observed values is about 20%–25%. Model results for cloudy skies could be improved with better estimates of cloud albedo and by accounting for multiple cloud layers.

Acknowledgments. We would like to acknowledge the assistance of Laura Easter and J.-Y. Kim in the preparation of this article. B. J. Sohn and Dr. M. V. K. Sivakumar provided satellite and radiation data for the project. The Meteorological Service of Niger provided cloud and visibility data. We would also like to thank Brent Holben for valuable discussions of the project.

APPENDIX

List of Symbols (in addition to those contained in Tables 1 and 2)

Symbol	*Description*
A_c	bulk cloud albedo
A_0	planetary or top albedo for clear skies

A^*_{obs} observed mean planetary albedo
A' mean cloud albedo of individual cloud type
a wavelength exponent
$amt_{k,i}$ amount of cloud type i during season k
c cloud cover (percent)
d earth–sun distance (km)
e vapor pressure (mb)
F_c ratio of downward to upward scattering
$f_{k,i}$ frequency of occurrence of cloud type i during season k
G^*_c global radiation under cloudy skies
G^*_0 global radiation under clear skies
G^*_{obs} observed monthly mean global radiation
H sunrise hour angle (radians)
H^*_0 absorption by the atmosphere under clear skies
I_0 solar constant (W m^{-2})
i cloud type index
k season index
M relative optical air mass
M' pressure-corrected optical air mass
M'_{co_2} pressure-corrected optical path length of carbon dioxide (cm)
M'_{o_3} pressure-corrected relative optical path length of ozone (cm)
M'_w pressure-corrected relative optical path length of water vapor (cm)
N total number of cloud types
p surface pressure (mb)
r carbon dioxide concentration (ppm)
T temperature (K)
u ozone content (cm)
VV horizontal visibility (km)
w precipitable water (cm)
w' water vapor path length (cm)
$\tilde{w}$ aerosol single scattering albedo
α_a aerosol absorptivity
α_c bulk cloud absorptivity
α_{co_2} carbon dioxide absorptivity
α_0 total absorptivity under clear skies
α_{o_2} oxygen absorptivity
α_{o_3} ozone absorptivity
$\alpha^{uv}_{o_3}$ ozone absorptivity due to ultraviolet radiation
$\alpha^{vis}_{o_3}$ ozone absorptivity due to visible radiation
α_w water vapor absorptivity
α' mean cloud absorptivity of individual cloud type
β turbidity coefficient
δ solar declination
δ_a aerosol optical depth (cm)
θ solar zenith angle
λ wavelength (cm)
μ_c effective ratio of spaceward scattering to total scattering of beam radiation by the bulk cloudiness
μ' ratio of spaceward scattering to total scattering of beam radiation of individual cloud type
σ_a scattering by aerosols
σ_c bulk cloud scattering
σ_0 total scattering under clear skies
σ_R Rayleigh scattering
σ' cloud scattering by individual cloud type
γ_a aerosol transmissivity
ϕ latitude

REFERENCES

Abdellaoui, A., F. Becker and E. Olory-Hechinger, 1986: Use of Meteosat for mapping thermal inertia and evapotranspiration over a limited region of Mali. *J. Climate Appl. Meteor.*, **25,** 1489–1506.

Anthes, R. A., 1984: Enhancement of convective precipitation by mesoscale variations in vegetative covering in semiarid regions. *J. Climate Appl. Meteor.*, **23,** 541–554.

ben Mohamed, A., and J.-P. Frangi, 1983: Humidity and turbidity parameters in Sahel: A case study for Niamey (Niger). *J. Climate Appl. Meteor.*, **22,** 1820–1823.

——, and ——, 1986: Results from ground-based monitoring of spectral aerosol optical thickness and horizontal extinction: Some specific characteristics of dusty Sahelian atmospheres. *J. Climate Appl. Meteor.*, **25,** 1807–1815.

Bird, R., and R. L. Hulstrom, 1981: Direct insolation models. *Trans. ASME J. Sol. Energy Eng.*, **103,** 182–192.

Brutsaert, W. H., 1982: *Evaporation into the Atmosphere: Theory, History and Applications.* D. Reidel, 299 pp.

Camillo, P. J., R. J. Gurney and T. J. Schmugge, 1983: A soil and atmospheric boundary layer model for evapotranspiration and soil moisture studies. *Water Resour. Res.*, **19,** 371–380.

Carlson, T. N., and S. G. Benjamin, 1980: Radiative heating rates for Saharan dust. *J. Atmos. Sci.*, **37,** 193–213.

——, J. N. Dodd, S. G. Benjamin and J. N. Cooper, 1981: Satellite estimation of the surface energy balance, moisture availability and thermal inertia. *J. Appl. Meteor.*, **20,** 67–87.

Cerf, A., 1980: Atmospheric turbidity over West-Africa. *Contrib. Atmos. Phys.*, **53,** 414–429.

——, Y. Fouquart, D. Bonnel, G. Brogniez, M. Chaoui-Roquai and L. Smith, 1982: Propriétés radiatives des aerosols saheliens. *La Météorologie VI^e*, **29,** 247–260.

Charney, J., 1975: Dynamics of deserts and drought in the Sahel. *Quart. J. Roy. Meteor. Soc.*, **101,** 193–202.

——, W. J. Quirk, S. H. Chow and J. Kornfield, 1977: A comparative study of the effects of albedo change on drought in semiarid regions. *J. Atmos. Sci.*, **34,** 1366–1385.

Cochemé, J., and P. Franquin, 1967: An agroclimatology survey of a semiarid area in Africa south of the Sahara. Tech. Note #86, WMO-#210.TP.110, 136 pp.

Corio, L. A., and R. T. Pinker, 1987: Estimating monthly mean water and energy budgets over the central U.S. Great Plains. Part II: Evapoclimatonomy experiments. *Mon. Wea. Rev.*, **115,** 1153–1160.

Courel, M. F., R. S. Kandel and S. I. Rasool, 1984: Surface albedo and the Sahel drought. *Nature*, **307,** 528–531.

Dabberdt, W. F., and P. A. Davis, 1978: Determination of energetic characteristics of urban–rural surfaces in the greater St. Louis area. *Bound.-Layer Meteor.*, **14,** 105–121.

d'Almeida, G. A., 1986: A model for Saharan dust transport. *J. Climate Appl. Meteor.*, **24,** 903–916.

Deardorff, J. W., 1978: Efficient prediction of ground surface temperature and moisture with inclusion of a layer of vegetation. *J. Geophys. Res.*, **83,** 1889–1903.

Drummond, A. J., and J. R. Hickey, 1971: Large-scale reflection and absorption of solar radiation by clouds as influencing earth radiation budgets: New aircraft measurements. *Proceedings International Conference on Weather Modification,* Canberra, Australia, Aust. Acad. Sci. and Amer. Meteor. Soc., 267–276.

FAO, 1984: *Agroclimatological Data, Vol. I.,* Food and Agricultural Organization.

Fouquart, Y., B. Bonnel, G. Brogniez, J. C. Buriez, L. Smith, J. J.

Morcrette and A. Cerf, 1987: Observations of Saharan aerosols: Results of ECLATS field experiment. Part II: Broadband radiative characteristics of the aerosols and vertical radiative flux divergence. *J. Climate Appl. Meteor.*, **26,** 38–52.

Frohlich, C., and R. W. Brusa, 1981: Solar radiation and its variation in time. *Solar Physics,* **74,** 209–215.

Griffiths, J. F., 1972: World survey of climatology. Vol. 10. H. Landsberg, Ed., *Climates of Africa,* Elsevier, 604 pp.

Iqbal, M., 1983: *An Introduction to Solar Radiation.* Academic Press, 390 pp.

Kutzbach, J. E., 1980: Estimates of past climate at Paleolake Chad, North Africa, based on a hydrological and energy-balance model. *Quat. Res.*, **14,** 210–223.

Lacis, A. A., and J. E. Hansen, 1974: A parameterization for the absorption of solar radiation in the Earth's atmosphere. *J. Atmos. Sci.*, **31,** 118–133.

Lettau, H. H., 1969: Evapotranspiration climatonomy. I. A new approach to numerical prediction of monthly evapotranspiration, runoff, and soil moisture storage. *Mon. Wea. Rev.*, **97,** 691–699.

——, and M. W. Baradas, 1973: Evapotranspiration climatonomy. II: Refinement of parameterization, exemplified by application to the Mabacan watershed. *Mon. Wea. Rev.*, **101,** 636–649.

——, and K. Lettau, 1969: Shortwave radiation climatonomy. *Tellus,* **21,** 208–222.

——, and ——, 1975: Regional climatonomy of tundra and boreal forests in Canada. Climate of the Arctic. *Proceedings of the 24th Alaskan Science Conference,* Fairbanks, AAAS and Am. Meteor. Soc., 209–221.

——, and ——, Eds., 1978: Exploring the world's driest climate. IES Report 101, Center for Climatic Research, Institute for Environmental Studies, University of Wisconsin–Madison, 264 pp.

——, —— and L. C. B. Molion, 1979: Amazonia's hydrologic cycle and the role of atmospheric recycling in assessing deforestation effects. *Mon. Wea. Rev.*, **107,** 227–238.

Lettau, K., 1970: Radiation climate of New Delhi—Part I: Shortwave radiation. *Indian J. Meteor. Geophys.*, **21,** 31–42.

Liou, K.-N., 1976: On the absorption, reflection and transmission of solar radiation in cloudy atmospheres. *J. Atmos. Sci.*, **33,** 798–805.

London, J., R. D. Bojkov, S. Oltmans and J. E. Kelley, 1976: Atlas of the global distribution of total ozone, July 1957–June 1967. Report No. NCAR/TN-113+STR, National Science Foundation, Washington, DC, 276 pp.

Lunde, P. J., 1980: *Solar Thermal Engineering.* Wiley, 612 pp.

Mächler, M., 1983: Parameterization of solar irradiation under clear skies. M.A.Sc. thesis, University of British Columbia, Vancouver.

Malo, A. R., 1988: The relationship between the normalized difference vegetation index and rainfall in West Africa. M.S. thesis, Department of Meteorology, Florida State University, 100 pp.

Monteith, J. L., Ed., 1975: *Vegetation and the atmosphere.* Vol. 1: *Principles.* Academic Press, 278 pp.

Nicholson, S. E., 1985: Sub-Saharan rainfall 1981–84. *J. Climate Appl. Meteor.*, **24,** 1389–1391.

——, 1986: African drought: An example of the influence of land-surface properties on climate? *Proceedings ISLSCP Conference,* Rome, Italy, 405–410.

——, 1988: Land surface–atmosphere interaction: Physical processes and surface changes and their impact. *Prog. Phys. Geogr.*, **12,** 36–65.

——, and A. R. Lare, 1990: A climatonomic description of the surface energy balance in the Central Sahel. Part II: The evapoclimatonomy submodel. *J. Appl. Meteor.*, **29,** 138–146.

Norton, C. C., F. R. Mosher and B. Hinton, 1979: An investigation of surface albedo variations during the recent Sahel drought. *J. Appl. Meteor.*, **18,** 1252–1262.

Oguntoyinbo, J. S., 1970: Reflection coefficient of natural vegetation, crops and urban surfaces in Nigeria. *Quart. J. Roy. Meteor. Soc.*, **96,** 430–441.

Paltridge, G. W., and C. M. R. Platt, 1976: *Radiative Processes in Meteorology and Climatology.* Elsevier, 318 pp.

Pinker, R. T., and L. A. Corio, 1987: Estimating monthly mean water and energy budgets over the central U.S. Great Plains. Part I: Evapoclimatonomy model formulation. *Mon. Wea. Rev.*, **115,** 1140–1152.

Price, J. C., 1982: On the use of satellite data to infer surface fluxes at meteorological scales. *J. Appl. Meteor.*, **21,** 1111–1122.

Prospero, J. M., and R. T. Nees, 1986: Impact of the North African drought and El Niño on mineral dust in the Barbados trade winds. *Nature,* **320,** 735–738.

Redmond, K., 1980: An emissivity parameterization suitable for climate modeling. *Mon. Wea. Rev.*, **108,** 663–675.

Riordan, A. J., 1982: Formulation and testing of a climatonomic simulation of the microclimate of the dry valleys and of the Little America V station in Antarctica. *Bound-Layer Meteor.*, **24,** 295–329.

Robinson, G. D., 1962: Absorption of solar radiation by atmospheric aerosol as revealed by measurements from the ground. *Arch. Meteor. Geophys. Bioklim.*, Ser. B, **12,** 19–40.

Rockwood, A. A., and S. K. Cox, 1978: Satellite inferred surface albedo over northwestern Africa. *J. Atmos. Sci.*, **35,** 513–522.

Rodgers, C. D., 1967: The radiative heat budget of the troposphere and lower stratosphere. Rep. No. A2, Planetary Circulation Project, Department of Meteorology, M.I.T., 99 pp.

Sasamori, T., J. London and D. V. Hoyt, 1972: Radiation budget of the Southern Hemisphere. *Meteor. Monogr.*, No. 35, Amer. Meteor. Soc., 9–23.

Sellers, W. D., 1965: *Physical Climatology.* The University of Chicago Press, 272 pp.

Smith, E. A., and M. R. Smith, 1987: Atlas of earth radiation budget measurements from Nimbus 7 ERB (1979–1983). Department of Meteorology and Supercomputer Computations Research Institute, Florida State University, Library of Congress Card Catalogue No. 87-80077, 254 pp.

Spencer, J. W., 1971: Fourier series representation of the position of the sun. *Search,* **2,** 172.

Sud, Y. C., and M. J. Fennessy, 1984: A numerical study of the influence of evaporation in semiarid regions on the July circulation. *J. Climatol.*, **4,** 383–398.

Taconet, O., R. Bernard and D. Vidal-Madjar, 1986a: Evapotranspiration over an agricultural region using a surface flux/temperature model based on NOAA–AVHRR data. *J. Climate Appl. Meteor.*, **25,** 284–307.

——, T. Carlson, R. Bernard and D. Vidal-Madjar, 1986b: Evaluation of a surface/vegetation parameterization using satellite measurements of surface temperature. *J. Climate Appl. Meteor.*, **25,** 1752–1767.

Twomey, S., 1978: Influence of the aerosol on optical properties of clouds. *JOC Study Conference on Parameterization of Extended Cloudiness and Radiation for Climate Models,* Geneva, World Meteorological Organization, Appendix E, 20 pp.

Warren, S. G., C. J. Hahn, J. London, R. M. Chervin and R. L. Jenne, 1986: Global distribution of total cloud cover and cloud type amounts over land. NCAR/TN-273+STR, 230 pp.

Yamamoto, G., 1962: Direct absorption of solar radiation by atmospheric water vapor, carbon dioxide and molecular oxygen. *J. Atmos. Sci.*, **19,** 182–188.